References

Code

Energy Harvesting Techniques for Internet of Things

Submitted to
Dr. Samah
El-Shafiey
El-Tantawy

Cairo University – Faculty of Engineering

Electronics and Electrical Communications

Mainstream – First year

Ordinary Differential Equations and Mathematical Transformations – MTHG103E

Energy harvesting techniques for the Internet of Things (IoT)

Submitted for MTHG103E project

Under the supervision of Dr. Samah El-Shafiey El-Tantawy

Code	B.N.	Sec.	Name
91240510	34	2	عمر شريف السيد عبدالخالق
91240647	18	3	محمد حسام الصاوي عمران
91240804	13	4	مينا وائل تناغو فهمى سدراك
91240840	22	4	هشام السيد احمد محمد الطياري
91240841	23	4	هشام عبدالرحمن محمود محمد
91240862	30	4	يوسف ابراهيم شعبان عبدالسلام
91240881	33	4	يوسف طلعت فاروق احمد السيد
91240892	34	4	يوسف محمد ابراهيم سيد

Table of content

Energy harvesting techniques for the Internet of Things (IoT)

Abstract—Traditional IoT devices rely on limited power sources, which makes them inefficient for long-term deployment. Energy harvesting offers a sustainable solution for powering **IoT** devices by converting ambient energy sources such as solar, thermal, and vibrational energy into electricity. This reduces dependence on conventional power storage and enables long-term, self-sustaining operation. This study explores various energy harvesting scenarios and optimizes energy usage through duty cycling strategies.

1. Introduction

The Internet of Things (**IoT**) is transforming industries by enabling interconnected devices to collect, process, and transmit data without human intervention. From smart cities, Industrial automation, healthcare, and environmental monitoring, **as well as IoT** applications, are rapidly expanding. However, its reliance on traditional battery-powered solutions introduces significant challenges. Battery-powered **IoT** nodes require frequent maintenance, leading to high operational costs, downtime, and environmental concerns due to battery disposal. This challenge becomes even more critical in remote and large-scale deployments where battery replacement is impractical.

Several studies and reports highlight the limitations of conventional batteries and the potential benefits of energy harvesting. For example, Fitbit recalled **1.7** million Ionic smartwatches after reports of batteries overheating in **2022**, causing burns to **78** users. Despite ongoing complaints from **2018** to **2020**, Fitbit did not promptly report the issues to the Consumer Product Safety Commission, leading to a **$12.25** million fine in 2025 **[1]**. In addition, a survey by Aviva revealed that over half of **501** UK businesses experienced issues related to lithium-ion batteries, such as sparks, fires, and explosions. Specifically, **36%** reported overheating incidents, **19%** encountered sparking, **17%** experienced smoking, and approximately **13%** faced fires or explosions in the workplace **[2]**. Herston Burns Unit has experienced a significant increase in admissions due to injuries related to e-scooters, which are the leading cause of these admissions, responsible for **57%** of burn cases. Injuries range from minor burns to severe cases necessitating multiple surgeries. Many injuries result from lithium-ion battery explosions, leading to serious burns and, in some instances, fatalities **[3]**.

Energy harvesting (**EH**) has emerged as a promising alternative, allowing **IoT** devices to extract energy from ambient sources such as sunlight, thermal gradients, radio frequency waves, and mechanical vibrations **[4]**. By utilizing these naturally available energy forms, **EH**-based **IoT** systems aim to achieve self-sustaining operation with minimal human intervention and a safer experience. Despite its potential, energy harvesting presents several critical limitations that hinder its widespread adoption in practical **IoT** applications.

One of the major obstacles is the low energy conversion efficiency of existing **EH** technologies. The amount of power harvested is often insufficient to support continuous operation, especially in scenarios where energy availability fluctuates. Solar harvesting, for instance, depends on light intensity, making it unreliable in indoor environments or during nighttime. Similarly, vibrational energy sources provide inconsistent power output, limiting their ability to sustain high-performance **IoT** nodes.

Another key challenge is scalability and deployment feasibility. While **EH** solutions work in controlled environments, their effectiveness diminishes when deployed across diverse real-world conditions. **IoT** networks span a variety of settings, from industrial plants to agricultural fields, each with unique energy availability constraints. Designing a universal **EH** solution that adapts to different operational conditions remains a complex task.

The integration of EH technologies with existing IoT architectures is another unresolved issue. Wireless Sensor Networks (**WSNs**), a vital component of **IoT** ecosystems, rely on stable power sources to ensure continuous data transmission. Harvested energy, however, is often unpredictable, leading to network instability and communication failures. Efficient power management strategies are needed to optimize energy storage and distribution while maintaining seamless connectivity.

In addition to these technical challenges, security and data processing must also be considered. **EH**-powered IoT devices typically operate with minimal energy reserves, limiting their computational capabilities. This restriction makes it difficult to implement robust security protocols, leaving such devices vulnerable to cyber threats. Furthermore, efficient data processing techniques are necessary to ensure that limited power is utilized effectively without compromising performance.

It is known that **30%** of the energy in **IoT** devices is wasted **[6**]. With the continuous expansion of **IoT** sensors, big data generates a large amount of computational pressure and network transmission overhead. As a result, **IoT** devices can lead to significant energy consumption and waste, with many major data centers losing more than **$10,000,000** annually due to inefficiencies **[6]**. Energy management must therefore be the first factor considered when developing a fully integrated **IoT** strategy that maximizes productivity and ultimately achieves cost-saving objectives.

While advancements in energy storage technologies, adaptive power management, and machine learning-based optimization have shown promise, these solutions are still in their early stages. A comprehensive approach that addresses the trade-offs between energy efficiency, scalability, and system reliability is required for energy harvesting to become a viable power source for **IoT**. Understanding these fundamental challenges will pave the way for more resilient and autonomous **IoT** networks, ultimately driving the next phase of smart technology evolution.

2. Literature Review

2.1 Optimizing IoT Energy Efficiency with Deep Learning: A Case for Solar-Powered Systems [2025]

Authors: Steve Smith, Nisar Ahmad

Realizing the advantages of the deep learning methodology in **IoT** telecommunications through solar power, this research studies the development of energy-efficient **IoT** systems. It analyzes methods to eliminate fluctuations in energy as well as suboptimal power management through predictive modeling and suitable energy optimization techniques. This study focuses specifically on forecasting solar energy availability and optimizing energy usage with intelligent control systems.

Methods and Results:

The authors propose a system based on **RNNs** and **LSTM** models to forecast solar energy fluctuations, while **DRL** is used to optimize electric usage according to energy availability. This approach increases energy efficiency by **25%** and reduces total energy consumption by **30%** while improving system reliability through hybrid energy sources. Nonetheless, several drawbacks were explained. To begin with, deep-learning models are too power-hungry to be implemented on low-powered IoT devices. Secondly, hybrid energy systems alone are inefficient because of the lack of good optimization algorithms. Hence, decentralized and scalable energy management systems are needed to ensure large-scale implementation over **IoT** networks. **[7]**

2.2 RF-Energy Harvester and Its Applications in IOT [2023]

Hema Nagaraja

This study focused on **RF** energy harvesting as an alternative to enhance the lifespan of IoT devices in remote and inaccessible locations with an assistance setup. Power cast **P2110B RF** energy harvesting integrated circuits (**RF-EH IC**) and evaluation board (**P2110B-EVB**) were considered for performance evaluation over **IoT** powering requirements. The use of ambient **RF** signals would enable the study to avoid battery limitations while allowing power autonomy improvement in potential **IoT** applications with lower power demand applications.

Methodology and Findings:

This study undertakes a comparison **of different experimental verification and literature review** as a means of evaluating the performance of the **P2110B IC**. The comparison points out its advantages over other **RF-EH ICs** on **the high (2.0V-5.5V) voltage range and regulated output** for low-power IoT applications.
Experimental verification shows that the **P2110B-EVB can successfully power an IoT node**

(NodeMCU + DHT11 sensor) through harvested RF energy.

Some limitations are mentioned:

- **Dependent on the RF signal strength** (availability of **RF** sources affects efficiency).
- **Limited output current (50 mA),** thus restricting high-power **IoT** devices support.
- **Environment limitations such as interference**, distance from the **RF** source, and obstructions.
- **Lack of long-term performance data**, and real-world deployment feasibility is thus uncertain.

Implications and Future Work:

By using ODE models, it will **optimize the energy flows and integration of hybrid energy** to enhance the efficiency and sustainability of **IoT** devices. Therefore, validation of this approach using real-world deployment data and long-term performance analysis is essential.**[8]**

2.3 Investigation of Energy Harvesting Techniques for IoT Devices [2024]

Authors: Grace Adams, Harper Robinson, Ava Clark

Energy harvesting technologies are revolutionizing how we generate and utilize energy by capturing wasted or unused energy from various sources. Two promising approaches—thermal energy harvesting and kinetic energy harvesting—offer sustainable solutions to improve energy efficiency and reduce reliance on traditional power sources. This paper explores how these technologies can be applied in industrial, wearable, and urban environments, highlighting their potential to reduce energy waste, lower operational costs, and support eco-friendly innovations.

Thermal Energy Harvesting

According to a report by the U.S. Department of Energy (**2022**), industrial facilities can lose up to **20%** of their energy as waste heat. This represents a significant inefficiency in energy consumption, as this lost heat is not utilized effectively. Our technique addresses this issue by leveraging thermal energy harvesting, which is particularly applicable in environments with prevalent temperature differentials.

This technique is based on the Seebeck effect, where a voltage is generated in a thermocouple when its ends experience a temperature difference. We are particularly interested in thermoelectric generators (**TEGs**), which utilize this effect to convert waste heat from industrial machines or processes into usable electricity. By implementing **TEGs**, we can reduce operational costs while enhancing energy efficiency.

One promising application of **TEGs** is in IoT-based monitoring systems. In smart buildings, for example, TEGs can be used to track temperature variations and autonomously adjust heating and cooling systems, thereby reducing overall energy consumption. A study by Kumar et al. (**2023**) demonstrated that integrating **TEGs** into building management systems led to a **15%** reduction in energy consumption. Given their potential, thermal energy harvesting presents a sustainable and cost-effective solution for industries and environments characterized by temperature fluctuations.

Kinetic Energy Harvesting

One of the challenges of wearable devices is the frequent need for battery replacement, which limits their sustainability and convenience. Kinetic energy harvesting offers a solution by utilizing the motion of the human body to generate electricity. For example, a smartwatch equipped with this technology could harvest energy from wrist movements, providing power to sensors that monitor blood pressure, heart rate, and activity levels.

This concept is enabled by piezoelectric materials, which generate electricity when subjected to mechanical stress. The demand for such materials has grown significantly due to the increasing need for self-powered devices, particularly in healthcare and fitness applications. A study by Wang et al. (**2022**) demonstrated that integrating piezoelectric materials into smart textiles could generate sufficient energy to operate biometric sensors for heart rate and movement tracking.

Beyond wearables, kinetic energy harvesting has broader applications. For instance, foot traffic on streets can be used to generate electricity to power streetlights or public information displays. By harnessing mechanical energy from human activity, we can develop sustainable and eco-friendly power solutions for urban environments **[9]**.

2.4 IoT-Based Hybrid Renewable Energy System for Smart Campus [2021]

Authors: Ali Eltamaly, Majed Alotaibi, Abdulrahman Alolah, Mohamed A. Ahmed

Smart grids are the future of energy systems, and their success depends heavily on modern technologies like the Internet of Things (**IoT**). **IoT** helps make energy systems smarter by using sensors and devices to monitor and control power usage more efficiently. This is especially important for hybrid renewable energy systems (**HRES**), which combine different energy sources like solar and wind to provide clean and cost-effective power. However, integrating these systems into the grid isn't easy issues like voltage fluctuations and grid instability can arise. This paper explores how **IoT** can solve these challenges and proposes a four-layer architecture to make **HRES** integration smoother and more reliable.

Smart Grids and IoT Integration

The development of smart grids requires advancements in information and communication technologies (**ICT**) because these technologies enhance energy system efficiency and reliability. The Internet of Things (**IoT**) improves monitoring and control systems through the integration of sensors and actuators. IoT solutions provide efficient data management solutions for applications such as smart meters and distributed energy resources (**DERs**).

Hybrid Renewable Energy Systems (HRES)

Hybrid renewable energy systems (**HRES**) are crucial for upcoming power networks because they offer financial and environmental advantages while serving both residential and commercial sectors. The integration of hybrid renewable energy systems brings about technical difficulties such as voltage fluctuations and grid instability. Although communication networks play an essential role in maintaining HRES reliability, their research remains insufficiently explored.

Proposed IoT-Based Architecture

This work proposes an **IoT**-based architecture for integrating **HRES** into power distribution systems, consisting of four layers: The architecture consists of four main layers, which are power, data acquisition, communication network, and application layers **[10]**.

2.5 Smart Grid Management Enhanced by IoT Device Integration to Improve Energy Efficiency and System Reliability [2024]

Authors: Monica Kalbande, Yashika Gaidhani, Tejaswini Panse, Navnath B. Pokale, Madhuri A. Tayal, Mininath Bendre

The integration of Internet of Things (**IoT**) technology into smart grid management has become a critical enabler for improving energy efficiency and system reliability in renewable energy systems. By leveraging real-time monitoring, predictive maintenance, and advanced data analytics, **IoT** solutions address key challenges in solar and wind energy systems, such as operational inefficiencies, maintenance losses, and grid integration. This paper explores how **IoT**-driven innovations enhance the performance of solar and wind energy systems, contributing to a more sustainable and reliable energy future.

Solar Energy Systems

Solar power facilities must be monitored for optimum electricity output. This monitoring helps to restore economic power production from power plants by replacing defective solar panels, identifying contact issues, and addressing problems related to sludge accumulated on output-reducing panels and shaking wires. Research demonstrates that proactive monitoring enhances solar panel efficiency by as much as **20%** through the timely detection and resolution of problems. Maintenance problems account for approximately **30%** of solar energy production losses, which could be prevented through proper monitoring systems.

We recommend a machine-controlled Internet of Things (IoT), which is essentially an alternative energy-viewing device that enables automated alternative energy consumption from anywhere on the Internet. The global market for solar IoT solutions is projected to grow from approximately **$5** billion in **2020** to over **$20** billion by **2025**, reflecting the increasing adoption of smart technologies in energy management. We choose AT supercontrollers while focusing primarily on mega controllers to meet solar battery requirements.

.

Our system provides real-time monitoring of solar batteries and sends IoT system performance data through the internet. Automated monitoring systems show potential to cut maintenance expenses by **15%** to **25%** while reducing downtime and avoiding serious failures. Furthermore, real-time monitoring can decrease operational costs by up to **30%**, allowing for immediate responses to performance issues.

We habitually use **IoT** to send alternate energy parameters to the **IoT** server. It now displays these metrics in a user-friendly graphical user interface and alerts the user when the performance limit is reached. Systems like **IoT** have been shown to improve user engagement by providing intuitive interfaces that help users understand energy consumption patterns and performance metrics. This allows for easy remote observation of solar power plants while also ensuring optimal power production. Overall, these advancements contribute to a more sustainable and efficient energy landscape.

Wind Energy Systems

IoT technology significantly enhances wind microgrid management by enabling real-time monitoring, optimizing energy distribution, and improving reliability. Intelligent algorithms use historical and live data to forecast energy output, allowing for better integration with the grid. Demand response strategies adjust energy consumption based on wind availability, ensuring optimal resource use.

Energy storage systems like batteries and flywheels help balance supply and demand by storing excess wind energy and releasing it when needed. For instance, lithium-ion

batteries have an efficiency of **85–95%** and can store wind energy for several hours, while flywheels have a shorter duration but offer **85–90%** efficiency.
Additionally, blockchain technology enhances security and transparency in energy transactions, fostering trust in renewable energy markets. By leveraging **IoT**-driven control systems, wind energy microgrids can operate more efficiently, reducing costs and accelerating the transition to sustainable energy solutions.**[11]**

3. Mathematical Modeling and Methodology

3.2 Radio frequency energy harvesting using 'Power cast P2110B'

Power cast **P2110B** is an integrated circuit (**IC**) used in receiving very low Radio frequencies and harvest those frequencies to convert them into a good moderate **DC** output (**2.0V-5V**).

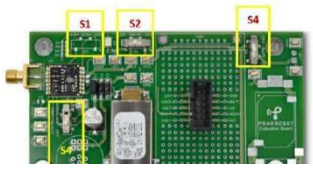

Figure 1: The P2110B [12]

3.2.1 P2110B's methodology

1. **Radio Frequencies input stage:** Radio frequencies are harvested from the environment using a **50 Ω** antenna to convert the radio frequency signals into **AC** signals
2. **Matching network:** A circuit used to match the impedance of the antenna to the impedance of the next circuit stage to achieve maximum power efficiency.
3. **Multi-stage rectifier:** After **AC** signals are collected, they get passed into a multistage rectifier specifically the **Dickson Charles pump (Charge pump)** model has multiple stages, **7** stages are used with each stage having diodes and capacitors which introduces non-linearity.
4. **Storage Capacitor:** The multi-stage rectifier charges an output capacitor to have a semi-regulated output.
5. **Maximum power point tracking and regulation:** The **IC** adjusts the operating point dynamically to maximize the power of the output.

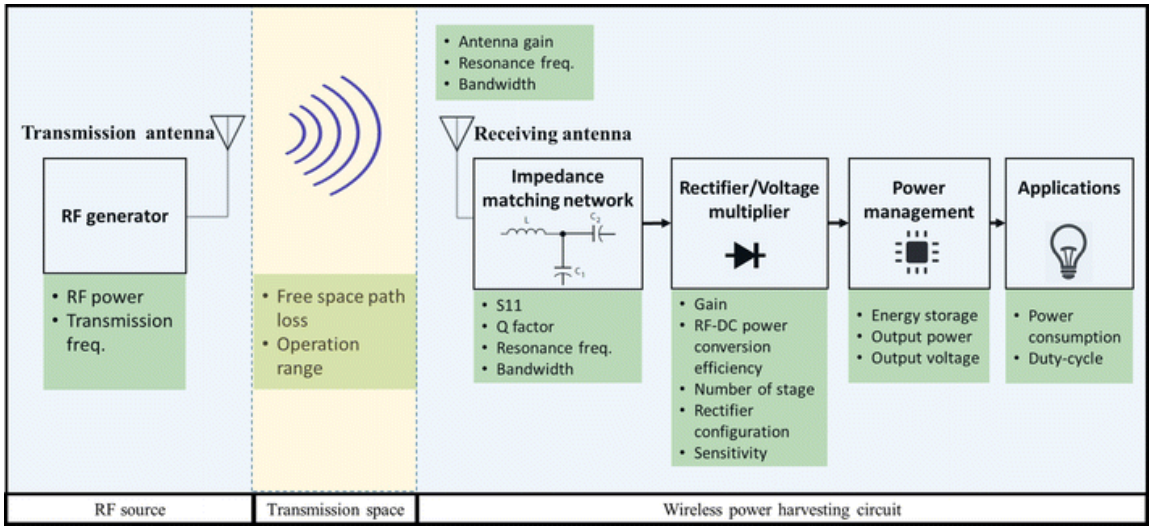

Figure 2: shows the stages of the P2011B [13]

3.2.2 The Transmission antenna

The antenna harvests radio frequency (**RF**) waves through electromagnetic coupling, with performance governed by near-field and far-field propagation dynamics. The system's behavior can be modeled as an **RLC** circuit. The system's response to Radiofrequency (**RF**) signals is described by the following equation

$$L_{ant}\frac{dI_{RF}(t)}{dt} + R_{ant}I_{RF}(t) = V_{RF}(t) \qquad (1)$$

where:

$\boldsymbol{I_{RF}(t)}$: The RF current induced in the antenna due to electromagnetic coupling

$\boldsymbol{V_{RF}(t)}$: The induced RF voltage at the antenna terminals.

$\boldsymbol{R_{ant}}$: The antenna resistance, representing the losses due to radiation and ohmic dissipation

$\boldsymbol{L_{ant}}$: The antenna inductance, which contributes to the system's impedance and resonance behavior.

By dividing equation (1) by $\boldsymbol{L_{ant}}$ we can rearrange it and write it as the following:

$$\frac{dI_{RF}(t)}{dt} + I_{RF}(t)\frac{R_{ant}}{L_{ant}} = \frac{V_{RF}(t)}{L_{ant}} \quad (2)$$

Since this corresponds to the general form of a linear differential equation, we can get an integrating factor by using its general formula:

$$e^{\int \frac{R_{ant}}{L_{ant}} dt} = e^{\frac{R_{ant}}{L_{ant}} t} \quad (3)$$

We can now write the equation as the following:

$$I_{RF}(t) e^{\frac{R_{ant}}{L_{ant}} t} = \int \frac{V_{RF}(t)}{L_{ant}} e^{\frac{R_{ant}}{L_{ant}} t} \, dt \quad (4)$$

By integrating the right-hand side and assuming that $\boldsymbol{V_{RF}(t) = V_0 \cos(\omega t)}$ we can represent the $\boldsymbol{I_{RF}(t)}$ as the following:

$$I_{RF}(t) = \frac{V_0}{Z_{ant}} \cos(\omega t - \phi) \quad (5)$$

This equation will help in determining:

- How much Radio frequency signals are harvested from the surroundings?
- The power is captured by knowing how much current is gained and flows into the circuit.
- Suitable RLC values for further modifications in the design of the circuit for maximum power efficiency.
- The quality of the antenna and how well it absorbs energy.

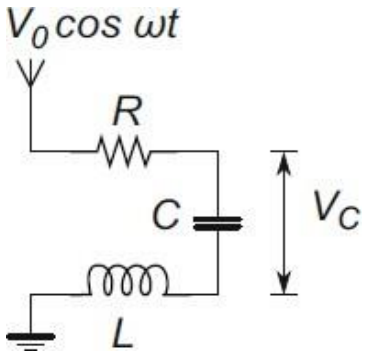

Figure 3: a simplified RLC model of the antenna [14]

3.2.3 The Matching Network

The matching network is modeled as an **RLC** circuit that takes its input from the antenna's output and adjusts the impedance of the antenna's output to match the impedance of the next stage to
get maximum power efficiency. This can be modeled through this equation:

$$L_m \frac{dI_m(t)}{dt} + \frac{1}{C_m} \int I_m(t)\ dt = V_{RF}(t) \tag{6}$$

where:

$\boldsymbol{L_m} = Matching\ network's\ inductance$

$\boldsymbol{C_m} = Matching\ network's\ capacitance$

$\boldsymbol{I_m(t)} = Matching\ network's\ current$

$\boldsymbol{V_{RF}(t)} = RF\ voltage\ input$

$\boldsymbol{Lm\ \frac{d\ Im(t)}{dt}} = Matching\ network's\ current$

$\boldsymbol{\frac{1}{C_m}\int I_m(t)\ dt} = RF\ voltage\ input$

By taking the derivative of this equation to eliminate the integral, we can get a second-order differential equation:

$$L_m \frac{d^2 I_m(t)}{dt^2} + \frac{1}{C_m} I_m(t) = \frac{dV_{RF}(t)}{dt} \tag{7}$$

This equation describes the behavior of the **RLC** circuit when it is excited by an external **RF** voltage, to solve it we need first to solve the left-hand side as a homogeneous equation:

$$L_m \frac{d^2 I_m(t)}{dt^2} + \frac{1}{C_m} I_m(t) = 0 \tag{8}$$

This equation can be solved and have a general solution that represents the current of the

matching network and demonstrates its relationship with the frequency.

$$I_m(t) = Ae^{j\omega_0 t} + Be^{-j\omega_0 t} \quad (9)$$

Where $\boldsymbol{\omega_0}$ is the resonance frequency where the frequency at the maximum power transfer occurs.

Assuming $\boldsymbol{V_{RF}(t)}$ *is a sinusoidal signal at some frequency* $\boldsymbol{\omega}$, we can say

$\boldsymbol{V_{RF}(t) = V_0 \cos(\omega t)}$ so we can get a particular solution for the right-hand side by using the method of undetermined coefficients to give us the following equation:

$$I_{particular}(t) = I_0 sin(\omega t) \quad (10)$$

The general solution of equation $(\mathbf{7})$ can be written as the following:

$$I_m(t) = Ae^{(j\omega_0 t)} + Be^{(-j\omega_0 t)} + I_0 sin(\omega t) \quad (11)$$

This equation represents the matching network's current at any frequency and demonstrates that at the resonance frequency, the current will be maximized so all energy from the antenna will be transferred into the next stage (rectifier stage) with minimum losses.

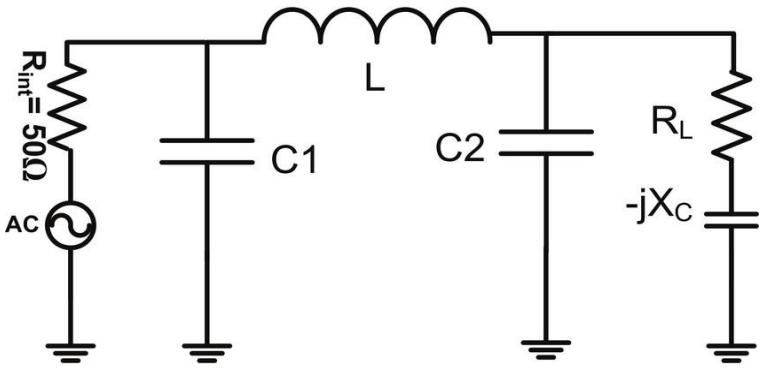

Figure 4: a simple model showing the matching network circuit [15]

3.2.4 The Multi-Stage Rectifier

After the signals are harvested by the antenna and then passed to the matching network circuit to ensure maximum power efficiency, the signals are now passed to the rectification stage to convert the signals from varying **AC** signals to **DC** signals, this can be shown in the following equation:

$$C_r \frac{dV_r(t)}{dt} + \frac{V_r(t)}{R_d} = I_m(t) \tag{12}$$

where:

$\boldsymbol{C_r} = rectifier\ capacitor(F)$

$\boldsymbol{R_d} = equivalent\ diode\ resistance(\Omega)$

$\boldsymbol{V_r(t)} = rectified\ voltage\ across\ capacitor(V)$

$\boldsymbol{I_m(t)} = input\ current\ from\ matching\ network(A)$

$\boldsymbol{C_r}\left(\frac{\boldsymbol{dV_r(t)}}{\boldsymbol{dt}}\right)$: *represents the capacitor's response, it demonstrates how fast the capacitor charges or discharges.*

$\frac{\boldsymbol{V_r(t)}}{\boldsymbol{R_d}}$: *represents the voltage leakage through the equivalent diode resistance* $\boldsymbol{R_d}$.

By dividing the equation by $\boldsymbol{C_r}$ we can get to the form of linear differential equations and get the following form:

$$\frac{dV_r(t)}{dt} + \frac{V_r(t)}{C_r R_d} = \frac{I_m(t)}{C_r} \tag{13}$$

We can get the integrating factor by the following equation:

$$e^{\int \frac{1}{C_r R_d} dt} = e^{\frac{t}{C_r R_d}} \tag{14}$$

By using the general form of the linear differential equation, we can get the equation to be like the following:

$$V_r(t)\, e^{\frac{t}{C_r R_d}} = \int \frac{I_m(t)\, e^{\frac{t}{C_r R_d}}}{C_r} dt \; + \; C \tag{15}$$

Assuming the current is constant DC instead of sinusoidal ($\boldsymbol{I_m(t)} = \boldsymbol{I_o}$ where I_o is the

maximum current amplitude) for the sake of simplicity, and assuming at **t = 0, V = V_o** (where V_o is the initial voltage on the capacitor). We can solve the equation as the following:

$$C = V_o - I_o R_d \tag{16}$$

$$V_r(t) = I_0 R_d \left(1 - e^{\frac{-t}{C_r R_d}}\right) + V_o \, e^{\frac{-t}{C_r R_d}} \tag{17}$$

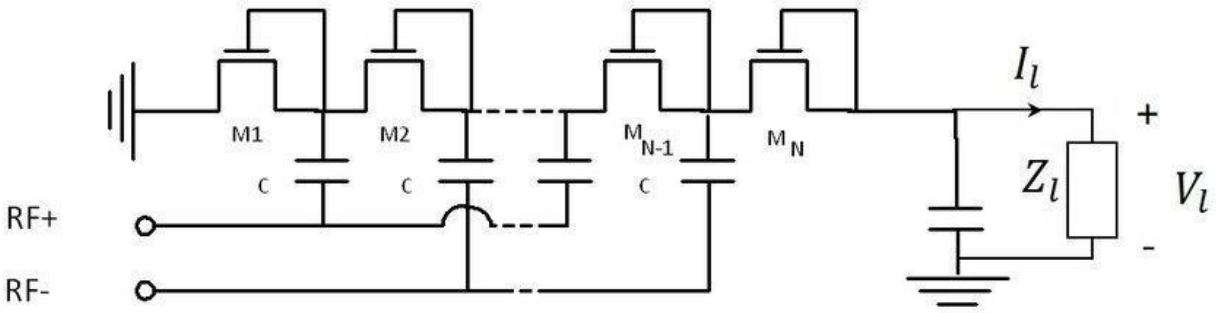

Figure 5: Dickson multi-stage rectifier model [16]

3.2.5 Load power consumption

After passing the Radio frequency signals through multiple stages to ensure stability and maximum efficiency, the last stage is the energy being passed to a storage capacitor and then to

determine whether the energy harvested is enough to operate the load or more harvesting is needed, this can be shown by the following equation:

$$P_L(t) = \frac{{V_c}^2(t)}{R} \tag{18}$$

As the capacitor charges and discharges with time, therefore the V_c is not constant and it can be described with the following equation:

$$C_s \frac{dV_c(t)}{dt} + \frac{V_c(t)}{R_L} = I_r \tag{19}$$

where:

$$\boldsymbol{C_s} = \textit{Storage capacitor}(F)$$
$$\boldsymbol{V_c(t)} = \textit{Capacitor voltage}(V)$$
$$\boldsymbol{R_L} = \textit{Load resistance}(\Omega)$$
$$\boldsymbol{I_r} = \textit{Rectified current}(A)$$
$$\frac{\boldsymbol{dV_{C(t)}}}{\boldsymbol{dt}} : \textit{Rate of change}(V/s)$$

Since this equation is pretty much the same as equation (12) we can directly substitute the $\boldsymbol{V_c(t)}$ expression to get the following equation:

$$P_L(t) = I_r^2 R_L \left(1 - 2e^{\frac{-t}{R_L C_s}} + e^{\frac{-2t}{R_L C_s}}\right) \tag{20}$$

4. Simulations and Experiments

Efficiency Analysis of RF-to-DC Conversion in Energy Harvesting Systems Using Different Modulation Schemes

Abstract

This study evaluates the efficiency of radio frequency (**RF**) to direct current (**DC**) power conversion using the Powercast **P2110B** energy harvesting device under various digital modulation schemes, including **16- QAM**, **PAM**, **BPSK**, **QPSK**, and **FSK**. The experiments were conducted at a carrier frequency of **915** MHz, with modulated signals generated via a Universal Software Radio Peripheral (**USRP**) controlled by **LabVIEW**. The harvested energy was measured at multiple receiver locations to analyze the impact of
distance and modulation type on conversion efficiency. Results demonstrate that **BPSK** modulation achieves the highest **RF**-to-**DC** conversion efficiency, outperforming other schemes across varying distances. These findings highlight the significance of modulation selection in optimizing energy harvesting for low-power wireless applications.

Introduction

Wireless energy harvesting (**WEH**) leverages ambient **RF** signals to power autonomous devices, offering a sustainable alternative to traditional batteries. Unlike solar or thermal energy, **RF** energy is controllable
and environment-independent, making it ideal for **IoT** and sensor networks. However, conversion efficiency depends heavily on the input waveform characteristics, including modulation type. Prior
research has explored waveforms like **OFDM** and chaotic signals, but the relationship between standard modulation schemes (e.g., **QAM**, **PSK**) and harvesting efficiency remains underexamined. This work bridges that gap by empirically evaluating five modulation schemes using a commercial energy harvester.

4.1 TRANSMISSION SYSTEM ARCHITECTURE

A standard personal computer serves as the foundation for wireless data transmission in this study. The system employs the **NI-USRP (National Instruments Universal Software Radio Peripheral)**, a software-defined radio (**SDR**) platform developed by National Instruments. The host computer interfaces with the USRP hardware via an Ethernet connection, enabling seamless transmission and reception of RF signals. **Key Components**:

1. **Software Control:**

   The system is programmed using **LabVIEW (Laboratory Virtual Instrument Engineering Workbench)**, a graphical development environment by National Instruments. LabVIEW facilitates the design, modulation, and real-time control of transmitted waveforms.

2. **Hardware Setup:**

   The **USRP 2G20** (Fig. 6) acts as the **RF** front-end, converting digital baseband signals from the host PC into analog waveforms at the target frequency (**915** MHz in this study)

Figure 6: NI-USRP 2920 hardware setup.

Signal Transmission Protocol

The wireless transmission process is implemented through a structured sequence of LabVIEW Virtual Instruments (**subVIs**), as illustrated in Figure 1. This systematic approach ensures proper initialization, configuration, and execution of the signal transmission:

1. **Initialization Phase (Initialize subVI)**
   - Establishes a software reference to the **NI-USRP** hardware.
   - Verifies successful host-hardware connection.
   - Performs system readiness checks before transmission.

2. **Configuration Phase (Configure subVI)**
   - Sets critical RF transmission parameters:
     - Antenna selection (TX/RX port activation).
     - IQ rate: **500** kHz (baseband sampling rate).
     - Carrier frequency: **915** MHz (ISM band).
     - Gain settings for optimal power output.
   - Configures hardware for specific modulation requirements.

3. **Signal Generation and Transmission (Start subVI)**
   - Initiates signal acquisition and processing.

   - Implements digital modulation schemes:
     - **Amplitude Modulation: PAM.**
     - **Phase Modulation**: BPSK, QPSK.
     - **Frequency Modulation: FSK.**
     - **Quadrature Modulation**: QAM.

   - Allows real-time parameter adjustment:
     - Samples per symbol.
     - PN sequence order.
     - Modulation type selection.

4. **Signal Monitoring (Read subVI)**
   - Captures IQ baseband signal samples
   - Provides real-time visualization:
     - Constellation diagrams
     - Time-domain waveforms.
     - Spectral characteristics.

5. Termination Sequence

- **Stop subVI**: Halts signal acquisition on command.
- **Close subVI**: Safely terminates hardware connection and releases system resources.

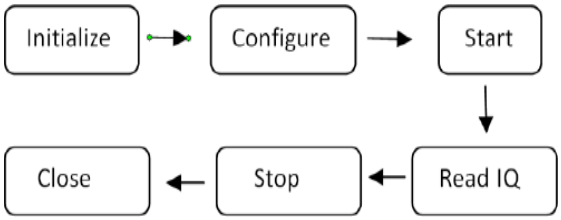

Figure 7: Steps involved in transmission

4.2 DEVELOPMENT OF ENERGY HARVESTING CIRCUIT

RF-to-DC Conversion System

The RF energy harvesting and conversion process is implemented using the Powercast **P2110B** power harvester module. This integrated solution offers several key features:

1. Device Characteristics

- Compact surface-mount (**SMD**) package design.
- Integrated RF energy harvesting and power management.
- Designed for battery-free, micropower applications.

2. Operation Principle

- Converts incident **RF** energy to **DC** power.
- Stores harvested energy in an external capacitor.
- Implements threshold-based voltage regulation:
  - Activates output when capacitor voltage reaches the upper threshold.
  - Deactivates output when the voltage falls below the lower threshold.
- Provides stable **DC** output voltage for connected loads.

3. Technical Context

This work builds upon an established energy harvester, where similar architectures have been successfully implemented for various low-power applications. The **P2110B** was selected for its:

- Proven reliability in RF energy harvesting applications.
- Compact form factor suitable for embedded systems.

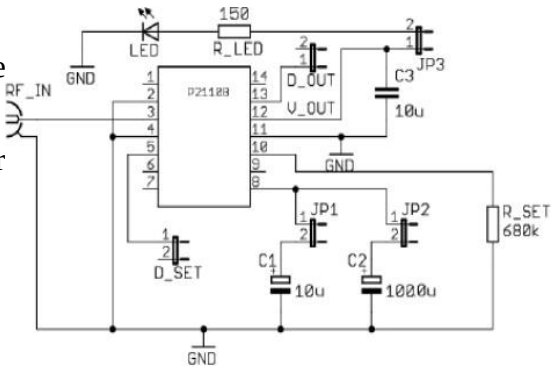

Figure 8: Circuit diagram of energy harvesting circuit

The circuit given in Fig.8. is developed using the respective hardware components and is shown in **Fig.9.**

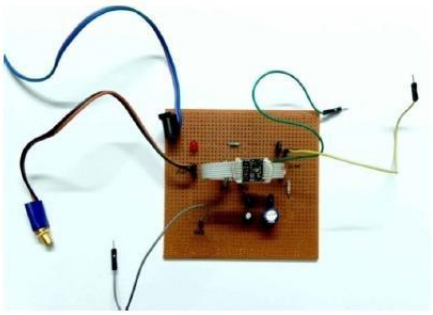

Figure 9: Hardware model of the circuit diagram

4.3 Description of experiment setup

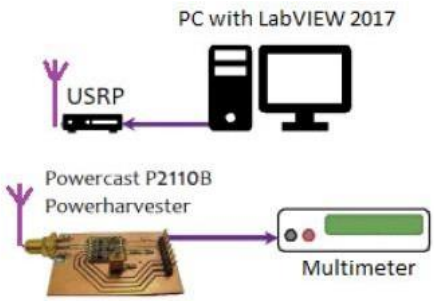

Figure 10: Experimental setup

Using the harvester circuit illustrated in Fig. **10** and the **LabVIEW** programs developed for various modulation schemes, the energy harvested from different waveform types was evaluated. Five modulation techniques were selected for this study: 16-**QAM**, **PAM**, **BPSK**, **QPSK**, and **FSK**. The experimental setup, adapted from **[17]**, is depicted in Fig. 11. The measurements were carried out in the Signal Processing and Image Processing laboratories at Thiagarajar College of Engineering, Madurai. Seven distinct receiver locations were identified within these labs to assess the harvested energy under varying spatial conditions.

Experimental Measurement Protocol

3. **Transmitter Configuration**
    - Primary transmission system consisting of:
        - Host computer running LabVIEW modulation programs
        - NI-USRP 2920 software-defined radio
        - Directional Yagi-Uda antenna (labeled Tx in Figure 5)
    - Transmitter parameters fixed at:
        - Center frequency: 915 MHz

4. **Receiver Deployment**

- Seven strategic measurement locations (R1-R7) were established as shown in Figure 6
- Location parameters varied systematically:
    - Distance gradient: 1.5m to 13.5m from Tx
    - Angular distribution: 0° to 110° relative to Tx orientation
    - Constant receiver antenna height maintained

5. **Measurement Procedure**

- The energy harvesting (EH) circuit is positioned at each location sequentially
- For each modulation scheme (16-QAM, PAM, BPSK, QPSK, FSK):
  a) Transmitter activated with specific modulation
  b) Allowed 30-second stabilization period
  c) Recorded output voltage at 1-second intervals for 2 minutes
  d) Calculated average harvested power using $P = V^2/R$ ($R=150\Omega$)

6. **Environmental Controls**

- Laboratory conditions maintained at:
    - Temperature: 25°C ± 2°C
    - Relative humidity: 50% ± 5%
    - Minimal RF interference verified via spectrum analysis

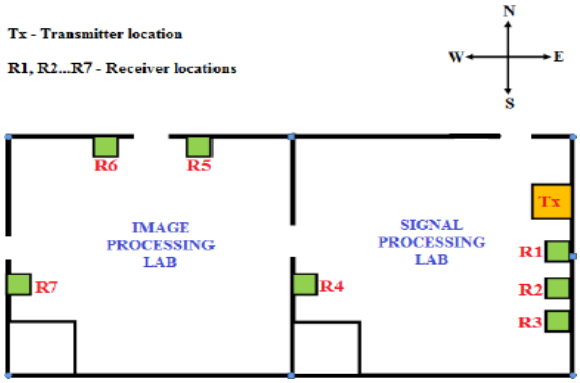

Figure 11: Map showing the locations where the transmit and receive antenna are placed.

Figure 12: Experimental setup with the transmitter and receiver at a Distance of 1.5 meters

5. Results and Discussions

The different signal-modulated schemes in the following Pictures are transmitted and received through USRP at a carrier frequency of **915 MHz**.

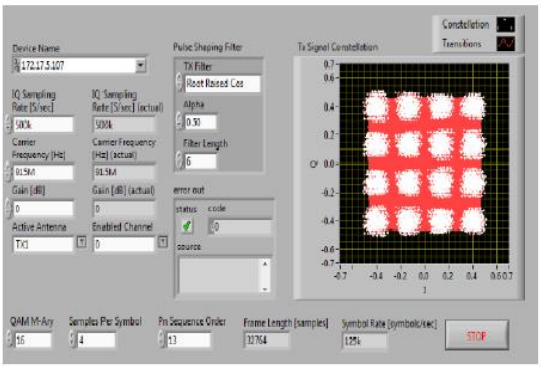

Figure 13: QAM Transmitter

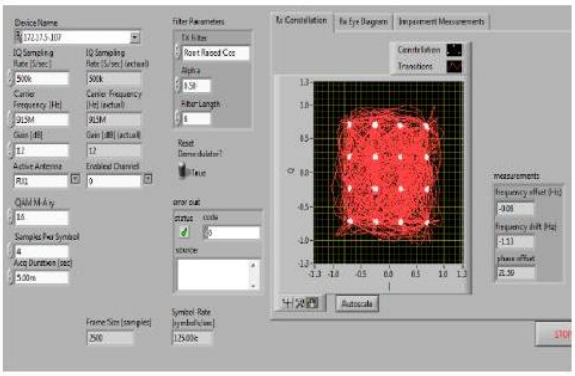

Figure 14: QAM Receiver

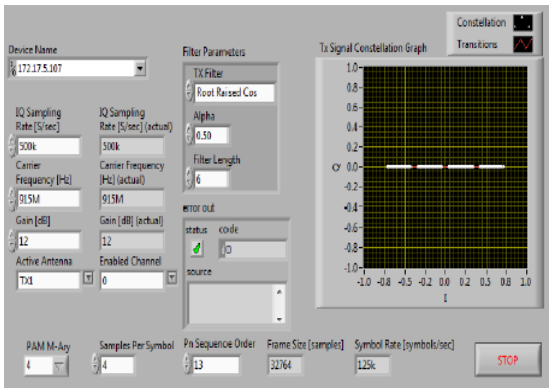

Figure 15: PAM Transmitter

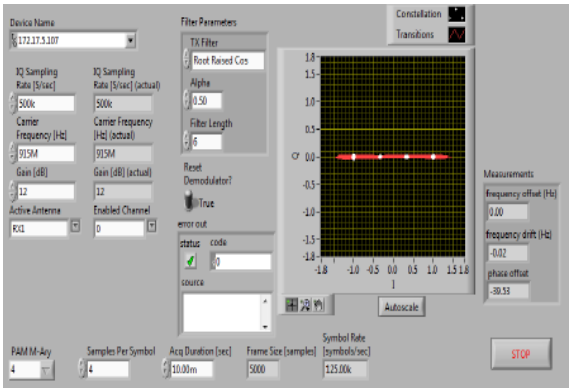

Figure 16: PAM Receiver

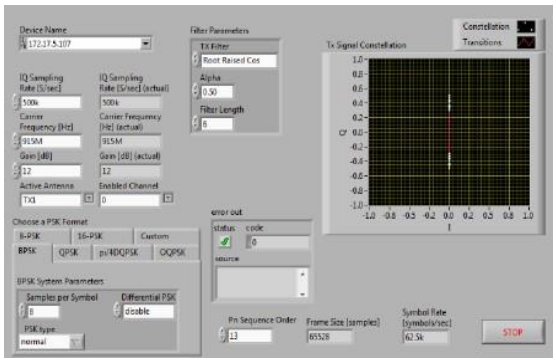

Figure 17: BPSK Transmitter

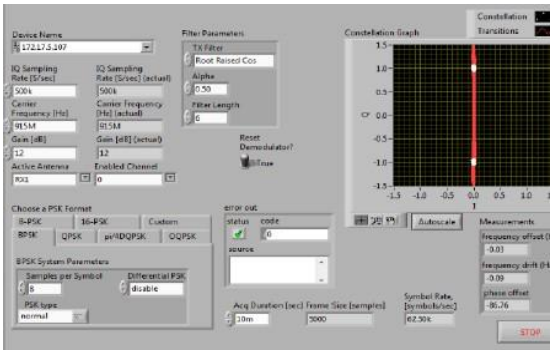

Figure 18: BPSK Receiver

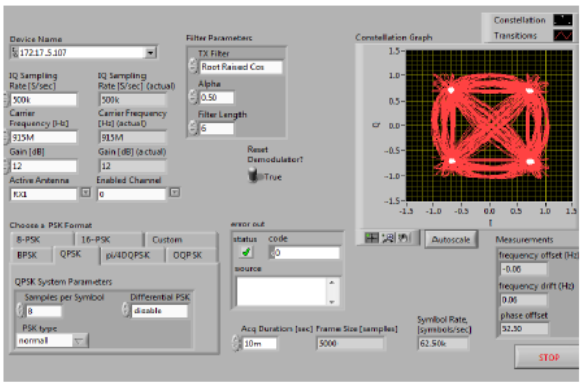

Figure 19: QPSK Transmitter

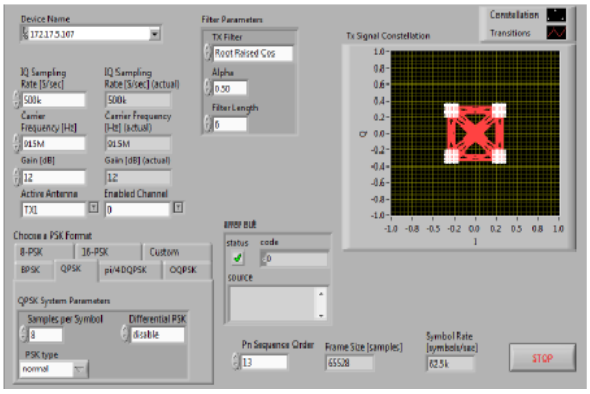

Figure 20: QPSK Receiver

The constellation diagrams indicate that the transmitted and received waveforms closely match. For energy harvesting measurements, the **USRP** module at the receiver end was replaced with the energy harvesting circuit at designated locations as shown in **Fig. 12.**

TABLE 1. POWER HARVESTED FOR 16-QAM SIGNAL

Location no.	Distance of the location from the transmitter (in metres)	Angle of the location from the transmitter (in degrees)	Mea-sured voltage (mV)	Harvest-ed power $P=V^2/R$ (µWatts) (R = 150 ohm)
R1	1.5	0	190	240
R2	2.5	0	170	192
R3	4	0	150	150
R4	7	55	120	96
R5	9	100	100	66
R6	11.5	110	90	54
R7	13.5	60	80	42

TABLE 2. POWER HARVESTED FOR PAM SIGNAL

Loc-ation no.	Distance of the location from the transmitter (in meters)	Angle of the location from the transmitter (in degrees)	Measur ed voltage (mV)	Harveste d power $P=V^2/R$ (µWatts) (R = 150 ohm)
R1	1.5	0	180	216
R2	2.5	0	160	170
R3	4	0	150	150
R4	7	55	120	96
R5	9	100	100	60
R6	11.5	110	80	42
R7	13.5	60	70	32

TABLE 3. POWER HARVESTED FOR BPSK SIGNAL

Loc-ation no.	Distance of the location from the transmitter (in meters)	Angle of the location from the transmitte r (in degrees)	Meas-ured voltage (mV)	Harves-ted power $P=V^2/R$ (µWatts) (R = 150 ohm)
R1	1.5	0	220	322
R2	2.5	0	200	266
R3	4	0	180	216
R4	7	55	150	150
R5	9	100	120	96
R6	11.5	110	110	80
R7	13.5	60	90	54

TABLE 4. POWER HARVESTED FOR QPSK SIGNAL

Loc-ation no.	Distance of the location from the transmitter (in meters)	Angle of the location from the transmitter (in degrees)	Measured voltage (mV)	Harvested power $P=V^2/R$ (µWatts) (R = 150 ohm)
R1	1.5	0	210	294
R2	2.5	0	200	266
R3	4	0	170	192
R4	7	55	150	15
R5	9	100	120	96
R6	11.5	110	100	66
R7	13.5	60	80	42

TABLE 5. POWER HARVESTED FOR FSK SIGNAL

Loc-ation no.	Distance of the location from the transmitter (in meters)	Angle of the location from the transmitter (in degrees)	Measured voltage (mV)	Harvested power $P=v^2/r$ (µWatts) (r = 150 ohm)
R1	1.5	0	170	192
R2	2.5	0	150	150
R3	4	0	130	112
R4	7	55	100	66
R5	9	100	90	54
R6	11.5	110	80	42
R7	13.5	60	60	24

Tables 1 through **5** demonstrate that as the distance between the receiver and transmitter increases, the amount of harvested power decreases. This confirms an inverse relationship between harvested power and the receiver's distance from the transmitter.

Fig. 16 presents a graphical representation of how the harvested power varies with distance. The graph indicates that **FSK**-modulated signals result in the lowest energy harvesting performance compared to the other modulation schemes. Meanwhile, 16-**QAM** and **PAM** exhibit similar levels of harvested energy, particularly in intermediate receiver positions.

Among all schemes, **BPSK** proves to be the most efficient, delivering the highest harvested power of **322** µW at a **1.5**-meter distance. Even at the farthest tested location (**13.5** meters), **BPSK** maintains a relatively high output of **0.54** µW, outperforming the other schemes. Notably, at some receiver positions, **QPSK** achieves harvested power levels comparable to those of **BPSK**.

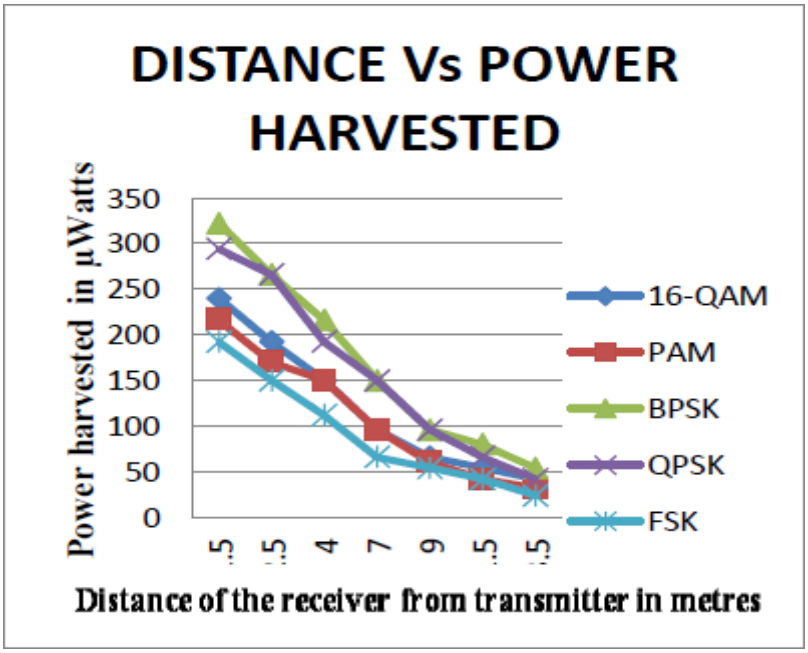

Figure 21: Graph showing the variation in the power harvested

Applications of the RF Energy Harvester (P2110B) [18]

The **Powercast P2110B Powerharvester** is a versatile energy harvesting module capable of enabling battery-free operation and supporting low-power devices across various fields. Below are some notable application areas:

A. Battery-Free Wireless Sensors

The **P2110B** serves as a critical enabler for **battery-free wireless sensor systems** across numerous domains. In **industrial monitoring** and **smart grids**, where continuous data acquisition is essential, and in **defense** and **building automation**, where reliable, maintenance-free power is necessary, the **P2110B** eliminates the dependency on traditional batteries. It is also especially valuable in **remote and harsh environments**, such as **oil and gas fields**, where access to power sources is limited. By efficiently converting ambient **RF** energy into usable power, the **P2110B** drives innovation in self-sustaining sensor networks.

B. Battery Recharging

The **P2110B** is well-suited for **recharging small-scale batteries**, including **coin cells** and **thin-film cells**. These battery types are commonly used in compact electronics and flexible applications, respectively. By providing a wireless and sustainable recharging method, the **P2110B** enhances battery longevity and usability, eliminating the need for frequent battery replacements and traditional charging methods.

C. Low-Power Electronics

The **P2110B** is particularly beneficial for **low-power electronic devices**, such as **remote sensors**, **wearables**, and **IoT gadgets**. It harvests **RF** energy and converts it into **DC** power, offering a reliable power supply for energy-efficient electronics. As the demand for **long-lasting, environmentally friendly electronics** grows.

V. Comparison with Other RF Energy Harvesting ICs [18]

In addition to Powercast's **P2110B**, several other companies such as **e-peas Semiconductors**, **RF Diagnostics**, and **Maxim Integrated** manufacture **RF energy harvesting integrated circuits (RF-EH ICs)**. A comparative overview is provided in **Table 1**, focusing on key performance metrics such as **output voltage**, **current capabilities**, **availability of evaluation boards**, and **battery compatibility**.

- The **AEM30940** from e-peas Semiconductors offers **1.8V to 4.2V** output and **20mA to 80mA** current.
- The **RFD102A** from RF Diagnostics delivers **40V** and **18mA**.
- Powercast's own **P1110B** provides **4.2V** output and **50mA** current.

These **ICs** can be selected based on the specific **voltage and current requirements** of the application. Given that popular IoT controllers like **Arduino** and **NodeMCU** operate in the **3.3V–5.5V** range, the **P2110B is an ideal choice**. Its evaluation board is especially suitable for research, development, and deployment in low-power, wireless **IoT** systems.

VI. Experiment Using the P2110B-EVB Evaluation Board

To demonstrate the practicality of the P2110B, an experiment was conducted where the **P2110B-EVB evaluation board** served as the power source for a **NodeMCU** microcontroller instead of a conventional battery.

Circuit Setup:

- The **V_{out}** and **GND** of the P2110B-EVB board were connected to the **V_{in}** and **GND** of the NodeMCU.
- A **DHT11 temperature and humidity sensor** was connected to the NodeMCU:
  - V_{CC} and GND → NodeMCU 3V3 and GND
  - Data pin → NodeMCU D4 pin

The **NodeMCU (ESP8266-based)** used its built-in Wi-Fi to connect to the **ThingSpeak** cloud platform. Data was transmitted using the following basic code:

```
const char *ssid = "XXXXXXXXXX";
const char *pass = "**********";
const char* server = "api.thingspeak.com";
```

A dedicated ThingSpeak channel was created using the **DHT11 write API key**, and the sensor data (temperature and humidity) was successfully uploaded. The channel statistics are visualized in **Figure 22**.

DHT11 sensor and NodeMCU in this setup are **not powered by a battery or direct-wired power** — instead, they are powered **only by RF energy**, harvested by the **P2110B-EVB** board.

This proves that **RF energy harvesting** can provide **enough power** to run a **wireless sensor system**, collect temperature and humidity data, and **transmit it to the cloud** (ThingSpeak).

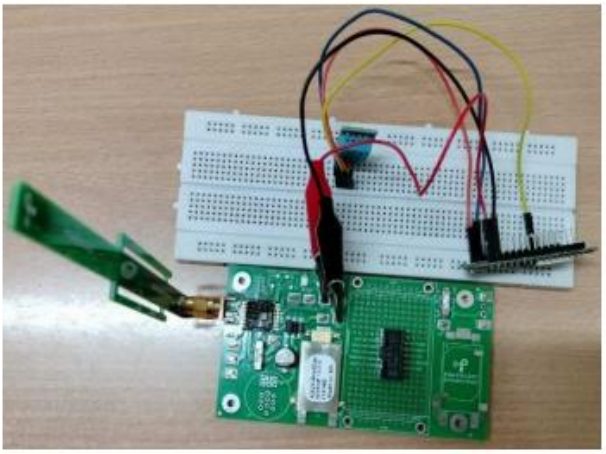

Figure 23: Power supply using P2110-EVB or as a power source

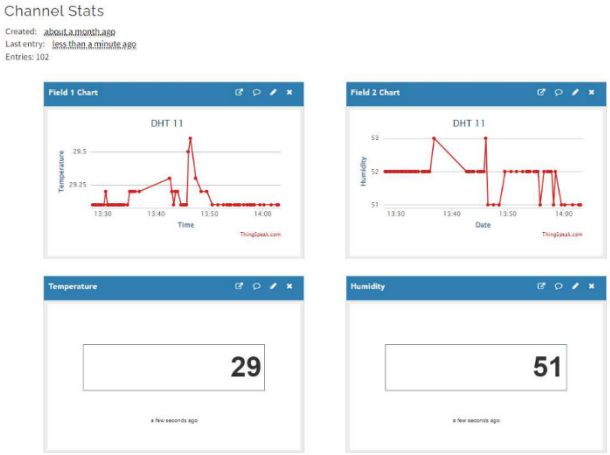

Figure 24: Temperature and humidity on ThingSpeak

6. Our contributions by using MATLAB

6.1 Purpose of the Circuit

This is an **RF signal strength detection system** that provides:

- An **analog output** (proportional to signal strength)
- A **digital output** (threshold-based detection)
- A **visual indicator (LED)** when signal exceeds a threshold

6.2 Major Components and Their Roles

PZ111B (Main IC)

- A monolithic **RF** power detector **IC**.
- Converts incoming **RF** signal into:
    - **Analog voltage (V_OUT)** = signal strength
    - **Digital logic (D_OUT)** = high if signal > threshold

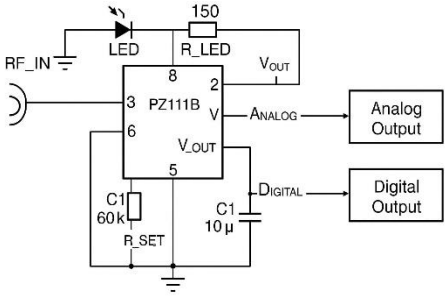

Figure 25: PZ111B Circuit

RF_IN

- Input for the **RF** signal (e.g., **433** MHz or **915** MHz).

- Comes from an antenna or **RF** module.
- The signal is fed into the chip's internal rectifier and envelope detector.

R_SET (Resistor)

- Connected to **Pin 5 (D_SET**).
- Sets the **threshold** for digital output (**D_OUT**).
    - Higher resistance = higher sensitivity (lower threshold).
    - In this schematic, a **60kΩ** resistor sets the threshold around **-5 dBm**.

C1 (10µF Capacitor)

- Smooths fluctuations at the digital output.
- Prevents false triggering due to signal noise or fast changes.

LED + R_LED (150Ω)

- Connected to the **analog output (V_OUT)**.
- Lights up when **RF** signal is strong enough to push **V_OUT** high.
- **R_LED** limits current to the **LED** (typical value is **150**–**330Ω**).

Analog Output (V_OUT)

- Proportional to input signal power.
- In the simulation: ~**0** V at **-30** dBm to ~**2** V at **+10** dBm.
- Can be connected to an **ADC** (Analog-to-Digital Converter) of a microcontroller.

Digital Output (D_OUT)

- A **binary signal**:
    - LOW (**0 V**) when signal < threshold (e.g., **-5 dBm**).
    - HIGH (**5 V**) when signal > threshold.
- Ideal for triggering an alarm, interrupt, or **LED**.

6.3 How the Circuit Works — Step by Step

1. **RF Signal Enters (RF_IN):**
    - The antenna captures an **RF** signal.
    - The signal is fed to **PZ111B**.

2. **RF Signal Processing Inside PZ111B:**
    - Internally, the **IC** rectifies and filters the **RF** signal.
    - It converts high-frequency **RF** power to a **DC** voltage.

3. **Analog Output (V_OUT):**
    - The internal detector outputs a **DC** voltage at **V_OUT** proportional to the log of **RF** input power.
    - This voltage drives the **LED** through **R_LED**.

4. **Digital Output (D_OUT):**
    - Based on the threshold set by **R_SET**, the chip compares signal strength.
    - If RF level > threshold → D_OUT goes **HIGH**.
    - Otherwise → D_OUT remains **LOW**.

5. **LED Behavior:**
    - When **V_OUT** is high enough (say > **1.6V**), it turns the **LED** on.
    - This gives a visual indication of detected **RF** power.

6.4 Our Results

1. Analog Output (V_OUT) vs. RF Input Power

- **Graph Description**:
  - The first plot shows the relationship between the **RF input power** (in dBm) and the **analog output voltage** (**V_OUT**) of the RF detector.
  - In this simulation, **V_OUT** is modeled as a **linear function** of **RF input power**. Specifically, the output voltage is scaled from 0V at -30 dBm to 2V at +10 dBm, based on the equation:

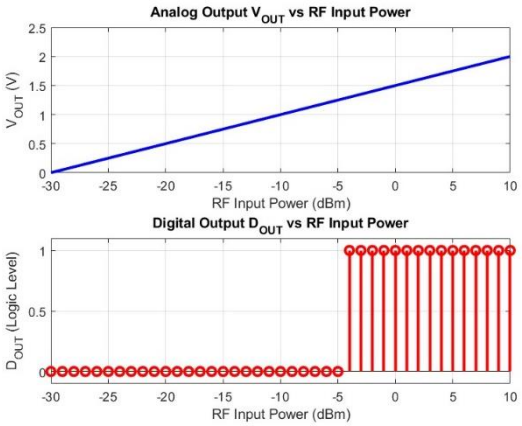

Figure 26: MATHLAB Results

$$V_{out} = \frac{2}{40}\,(rf_{dBm} + 30\,) \qquad (1)$$

  - **Key Observations**:
    - As the **RF input power** increases, the **analog output voltage** increases linearly from **0V** at -30 dBm to **2V** at +10 dBm.
    - This linear behavior is an idealized model and is not fully representative of real-world RF detectors, which typically have a **logarithmic relationship** between input power and output voltage.
  - **Real-World Consideration**:
    - In practical scenarios, RF detectors like the **PZ111B** exhibit a **logarithmic relationship** between input power and output voltage, meaning the output voltage changes more significantly at lower RF power levels and becomes less sensitive at higher power levels. This model is an approximation for simplicity and understanding.

2. Digital Output (D_OUT) vs. RF Input Power

- **Graph Description**:
    - The second plot shows the digital output (**D_OUT**) as a function of **RF input power**.
    - **D_OUT** is set to **1** (HIGH) when the RF input exceeds **-5 dBm**, and **0** (LOW) when it is below **-5 dBm**.
    - **Key Observations**:
        - The output remains **0** (LOW) for RF input powers ranging from -30 dBm to -5 dBm.
        - When the RF input power exceeds **-5 dBm**, **D_OUT** switches to **1** (HIGH), indicating the presence of a sufficient RF signal.
        - This plot illustrates the **threshold detection** capability of the detector, where the output transitions from LOW to HIGH at a specified RF input threshold.
    - **Real-World Consideration**:
        - In practical applications, digital RF detectors may have a similar threshold behavior, where the output switches from LOW to HIGH at a specific threshold power. However, the transition may not be as abrupt as in this simulation and may depend on the specific characteristics of the detector IC.

Conclusion

- **Analog Output**: The first graph shows a **linear relationship** between the RF input power and the output voltage. In real-world applications, RF detectors like the **PZ111B** typically have a **logarithmic** response.
- **Digital Output**: The second graph shows how the digital output changes based on a predefined threshold, switching from LOW to HIGH when the RF input power surpasses a certain level.

These results are simplified approximations to demonstrate the general behavior of RF power detectors. For more accurate modeling, a **logarithmic scale** should be used for the analog output to better represent the real-world behavior of the **PZ111B** RF detector IC.

7. RF Energy Harvesting: Antenna Design and Characteristics

Receiver antennas are a critical component in **RF** energy harvesting (**RFEH**) systems. Their primary function is to capture **RF** signals emitted from ambient or dedicated sources and significantly influence the overall conversion efficiency of the system. Optimizing the antenna for resonance at either single or multiple frequency bands is essential to maximize harvested power.

High-gain receive antennas are particularly important in applications requiring substantial power input, such as wireless charging of mobile devices, sensor wake-up systems, and wireless sensor networks (**WSNs**). These antennas must be capable of delivering sufficient power even in environments where **RF** energy is scarce.

Key characteristics of effective **RFEH** antennas include:

- **Power amplification** for stronger signal reception.
- **Wide bandwidth** to capture energy across various frequencies.
- **Miniaturization** while maintaining high efficiency.
- **Circular polarization** to reduce polarization mismatch losses and improve signal reception from diverse orientations

For biomedical applications, such as **wearable and implantable antennas**, additional design constraints come into play. These include:

- **Flexibility** for comfort and adaptability to body movements.
- **Durability** to withstand prolonged use.
- **Lightweight** to ensure user comfort.
- **Safety**, particularly regarding biocompatibility
- and minimal thermal impact on human tissue.

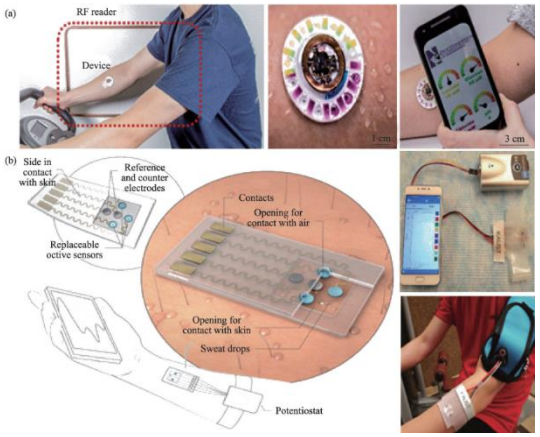

Figure 27: Wireless battery-free sweat sensor system for RF energy harvest with a smartphone Bluetooth wirelessly transmitter for analysis and monitoring. [20]

An example of such innovation is a **wireless battery-free sweat sensor system**, which monitors sweat composition in real-time. As shown in Figure 27, the system includes a multifunctional sweat sensor embedded in a wearable film. This film interfaces with an electrochemical analyzer, and the collected data is transmitted wirelessly to a smartphone via Bluetooth for continuous health monitoring and analysis. **[19]**

8. Beyond RF energy harvesting, which captures electromagnetic energy, other energy harvesting methods involve mechanical-to-electrical conversion will be discussed in the following sections [21]

Body-Integrated Self-Powered System for Wearable and Implantable Applications

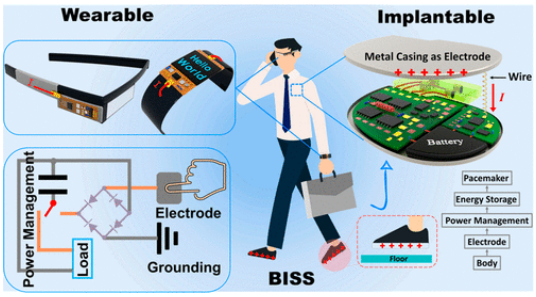

Figure 28: BISS demonstrative diagram

We present a body-integrated self-powered system (**BISS**) that offers a simple, highly efficient, and cost-effective method to harvest energy from human motion. Biomechanical energy generated by body movements is collected through an electrode attached to the skin. The fundamental working principle of the **BISS** is based on the combined effects of triboelectrification between the soles and the floor, and the electrification of the human body. We have demonstrated the feasibility of using **BISS** to power electronic devices through both in vitro and in vivo experiments. Our study shows that **BISS** provides an extraordinarily simple, economical, and practical approach for harvesting energy from body movements, highlighting its significant potential for future applications in self-powered wearable and implantable electronics.

Piezoelectric energy harvesting for self-powered wearable upper limb applications [22]

Piezoelectric energy harvesters work by converting vibration energy from human motion into useful electrical signals, making them ideal for powering on-body health monitoring devices. The energy harvesting unit uses a piezoelectric transducer to transform mechanical energy into electrical energy. The harvested energy can either be used immediately or stored in a reservoir such as a lithium-ion battery or a supercapacitor. The sensing unit acquires environmental data from the wearable, which is then processed by the signal processing unit. As shown in the figure, all these functional units can be powered by the energy scavenged through the piezoelectric energy harvester. This review focuses specifically on the energy harvesting block, where piezoelectric transducers are utilized to convert energy from human kinetic movements.

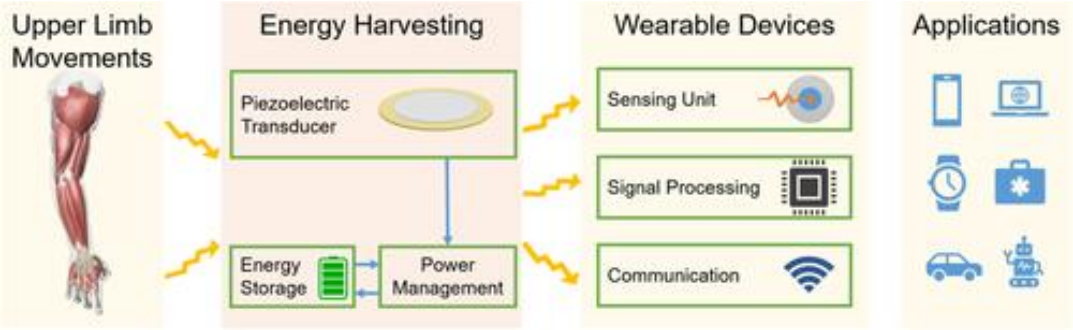

Figure 29: A building block of typical wearable device

Battery-Free Self-Powered Wearable System Using Triboelectric Nanogenerators [23]

Triboelectric nanogenerators (**TENGs**), which convert mechanical energy from human motion into electrical energy through a combination of triboelectric and inductive effects, present an appealing energy harvesting method for powering wearable sweat sensors—particularly during vigorous physical activity. Unlike solar or **RF**-powered devices, **TENGs** do not depend on inconsistent external energy sources. However, most existing **TENG**-based devices are hindered by limited power intensity, inefficient power management systems, and insufficient energy continuity, making them unsuitable for powering fully integrated, wireless, wearable molecular sensing platforms.

To address these challenges, we propose a fully self-powered, battery-free wearable system. This system integrates:

- A **freestanding-mode triboelectric nanogenerator (FTENG)**,
- **Low-power wireless sensor electronics**, and
- A **microfluidic sweat sensor patch**, all housed on a single **flexible printed circuit board (FPCB)** platform.

The device, referred to as **FWS³ (FTENG-powered Wearable Sweat Sensor System)**, enables dynamic monitoring of key sweat biomarkers such as **pH** and sodium ion concentration ($\mathbf{Na^+}$). Designed for compatibility with conventional FPCB fabrication processes, the system supports scalable production while maintaining high reliability. The freestanding structure of the **FTENG** allows for efficient energy harvesting directly from the skin's mechanical interactions, particularly effective

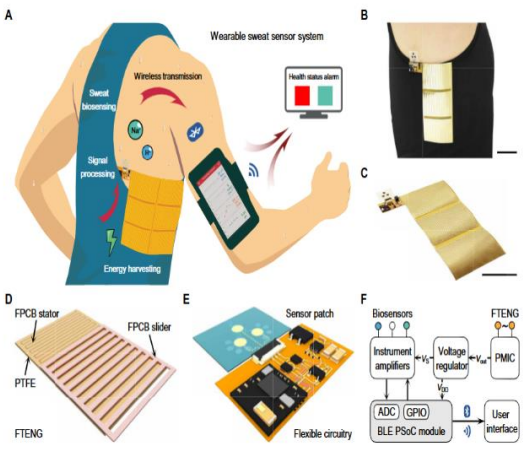

Figure 30

when laminated onto the side torso using waterproof medical tape.

A **Bluetooth Low Energy (BLE)** module is integrated for seamless transmission of sensor data to mobile devices, facilitating real-time health monitoring during exercise. This work represents the first demonstration of a fully integrated, battery-free, triboelectrically powered wearable platform capable of multiplexed sweat biomarker sensing.

On-Body Evaluation of the FWS³

During activities like running, rowing, or elliptical training, the sliding motion between the inner arm and torso creates an ideal condition for energy harvesting. In our tests, the **FTENG** stator was mounted on the torso while the slider was placed on the inner arm.

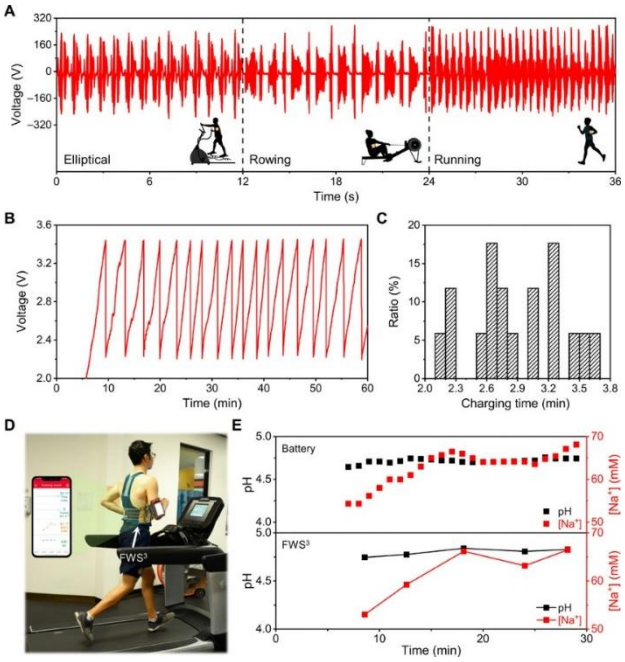

Figure 31

For validation, a treadmill running at a constant speed of **9** km/h was selected. The system's power generation during exercise is presented in Fig. **A**. During a **60**-minute run, the **FPCB** storage capacitor completed up to **18** full charge-discharge cycles (**Fig. B**), with each cycle lasting between **2.1** and **3.7** minutes (**Fig. C**). The FTENG generates electricity whenever the slider and stator make contact, and once the capacitor reaches a threshold voltage, it discharges to power a measurement event. Variability in the charging cycles is attributed to differences in contact area, force, and frequency of movement.

Performance evaluation involved placing two systems—one powered by **FTENG**, the other by a battery—on the subject's back. Both successfully transmitted data wirelessly via **BLE**. Five successful measurements were recorded over a **30**-minute period, during which stable **pH** levels and increasing **Na⁺** concentrations were observed, confirming the **FWS³** system's sensing accuracy (**Fig. E**).

These results highlight the potential of the **FWS³** as a reliable, self-powered platform for continuous, real-time monitoring of sweat-based physiological biomarkers during exercise.

9. Conclusion and Future work

LabVIEW block diagrams were used to transmit various modulated signals via the **USRP** platform, and energy was successfully harvested using the **Powercast P2110B** module. The harvested energy, initially obtained as voltage, was converted into power for detailed analysis. Among the tested modulation schemes, **BPSK** yielded the highest energy harvesting efficiency, though power decreased with increased distance between transmitter and receiver. This report also highlights the Powercast **P2110B's** ability to wirelessly power **IoT** devices, proving its value in real-world applications. Comparisons with other **RF** harvesting **ICs** and successful tests with **NodeMCU** further support its practicality. The study also explored alternative energy sources like body-integrated systems, piezoelectric devices, and triboelectric nanogenerators, each offering promising solutions for battery-free, self-powered wearable and implantable electronics. Together, these technologies represent a step toward more sustainable, maintenance-free electronic systems.

Artificial Intelligence (**Al**) is significantly enhancing energy harvesting systems by introducing intelligent algorithms that optimize energy prediction, control, and management. Techniques such as Artificial Neural Networks (**ANN**), Adaptive Neuro-Fuzzy Inference Systems (**ANFIS**), and Genetic Algorithms (**GA**) are increasingly used to improve the performance and adaptability of these systems.

ANNs, for example, are effective at predicting solar energy availability, enabling dynamic adaptation of the harvesting process for greater efficiency. **Al**-driven approaches are replacing traditional fixed algorithms with adaptive, self-learning methods that better handle environmental variability, resulting in improved reliability and overall system performance

10. REFERENCES

[1] "Fitbit Fined Over Ionic Smartwatch Burns." *The Verge*. [Online] Available: https://www.theverge.com/2025/1/23/24350413/fitbit-fine-ionic-smartwatch-burns.

[2] "Lithium-Ion Battery Incidents Affect More Than Half of Businesses." *Aviva*. [Online]. Available: https://gcs.aviva.com/en-gb/news/Lithium-ion-battery-incidents-affect-more-than-half-of-businesses/.

[3] "Herston Burns Unit Overwhelmed by E-Scooter and Vape Injuries." Wilston Grange News. [Online]. Available: https://wilstongrangenews.com.au/herston-burns-unit-overwhelmed-by-e-scooter-and-vape-injuries/.

[4] Teodora Sanislav, George Dan Mois, Sherali Zeadally, Silviu Corneliu Folea, "Energy Harvesting Techniques for Internet of Things (IoT)." *IEEE Access*, vol. 9, pp. 39530–39549, 2021.

[5] M. Alioto, E. Bonizzoni, F. Crupi, and D. De Caro. "Energy Harvesting Technologies for IoT Edge Devices." *IEEE Journal on Emerging and Selected Topics in Circuits and Systems*, vol. 8, no. 4, pp. 774–786, Dec. 2018.

[6] Shah, S., Jadeja, A., & Doshi, N. "An Analytical Survey of Energy Efficiency in IoT Paradigm." *Proceedings of the 3rd International Workshop on Internet of Things: Scope and Opportunities (IoT-S&O 2022)*, Leuven, Belgium, Oct. 26-28, 2022.

[7] ResearchGate, "Solar Energy for IoT," *ResearchGate Publications*. [Online]. Available: https://www.researchgate.net/search.Search.html?query=Solar+Energy+for+IoT&type=publication

[8] "RF-Energy Harvester and Its Applications in IoT: A Review," *ResearchGate Publications*, 2023. [Online]. Available: https://www.researchgate.net/publication/378082885_RF-Energy_Harvester_and_Its_Applications_in_IoT_A_Review

[9] Grace Adams, Harper Robinson, Ava Clark," Investigation of Energy Harvesting Techniques for IoT Devices," IJMICSE [Online]. Available: https://international.aritekin.or.id/index.php/IJMICSE/article/view/71

[10]" Smart Grid Management Enhanced by IoT Device Integration to Improve Energy Efficiency and System Reliability," [Online]. Available: https://internationalpubls.com/index.php/pmj/article/view/1866

[11] Ali Eltamaly, Majed Alotaibi, Abdulrahman Alolah, Mohamed A. Ahmed, "IoT-Based Hybrid Renewable Energy System for Smart Campus," *ResearchGate Publications*, 2021. [Online]. Available: https://www.researchgate.net/publication/353611601_IoT-%20Based_Hybrid_Renewable_Energy_System_for_Smart_Campus

[12] A. Kaur and H. Nagaraja, "RF-energy harvester and its applications in IoT: A review," in *2023 Second International Conference on Informatics (ICI)*, Nov. 2023. DOI: 10.1109/ICI60088.2023.10421418.

[13] L.-G. Tran, H.-K. Cha, and W.-T. Park, "RF power harvesting: A review on designing methodologies and applications," *Micro and Nano Systems Letters*, vol. 5, no. 14, 2017, Art. no. 14. DOI: 10.1186/s40486-017-0051-0.

[14] *EE Diary*, "How antenna as RLC circuit works," *EE Diary*, Jun. 2023. [Online]. Available: https://www.ee-diary.com/2023/06/how-antenna-as-rlc-circuit-works.html#google_vignette.

[15] J. Singh, "Performance analysis of RF energy harvesting circuit with varying matching network elements and diode parameters," Sep. 2015. DOI: 10.13140/RG.2.1.4838.4488.

[16] H. Rahmani, "Integrated electromagnetic wireless power harvesting system for mm-size biomedical implants," Apr. 2017. DOI: 10.13140/RG.2.2.32007.04000.

[17] C. R. Reddy, K. S. Reddy, and S. R. Reddy, "Design and implementation of a low power RF energy harvesting system for wireless sensor networks," in *Proc. Int. Conf. Recent Advances in Energy-efficient Computing and Communication (ICRAECC)*, Nagercoil, India, Mar. 2019, pp. 1–5, DOI: 10.1109/ICRAECC43874.2019.8995099.

[18] A. Kaur and H. Nagaraja, "RF-Energy Harvester and Its Applications in IoT: A Review," in Proc. 2023 Second Int. Conf. Informatics (ICI), Nov. 2023, DOI: 10.1109/ICI60088.2023.10421418.

[19] E. D. Nwalike, K. A. Ibrahim, F. Crawley, Q. Qin, P. Luk, and Z. Luo, "Harnessing Energy for Wearables: A Review of Radio Frequency Energy Harvesting Technologies," Energies, vol. 16, no. 15, p. 5711, Jul. 2023, DOI: 10.3390/en16155711.

[20] Y. Li, L. Zheng, and X. Wang, "Flexible and wearable healthcare sensors for visual reality health-monitoring," Virtual Reality & Intelligent Hardware, vol. 1, no. 4, pp. 386–404, Aug. 2019, DOI: 10.1016/j.vrih.2019.08.001.

[21] B. Shi et al., "Body-integrated self-powered system for wearable and implantable applications," ACS Nano, vol. 13, no. 5, pp. 6017–6024, May 2019, DOI: 10.1021/acsnano.9b02233.

[22] Y. Liu, H. Khanbareh, M. A. Halim, A. Feeney, X. Zhang, H. Heidari, and R. Ghannam, "Piezoelectric energy harvesting for self-powered wearable upper limb applications," Nano Select, vol. 2, no. 9, pp. 1762–1779, Feb. 2021, DOI: 10.1002/nano.202000242.

[23] Y. Song, J. Min, Y. Yu, H. Wang, Y. Yang, H. Zhang, and W. Gao, "Wireless battery-free wearable sweat sensor powered by human motion," Science Advances, vol. 6, no. 40, p. eaay9842, Sep. 2020, DOI: 10.1126/sciadv.aay9842.

11. Appendix

```
% RF Detector Simulation (PZ111B Behavior Approximation)

% RF Input Power Range (in dBm)

rf_dBm = -30:1:10;

% Analog Output (V_OUT) Model: linearly mapped from 0V (-30dBm) to 2V
(+10dBm)

V_OUT = (rf_dBm + 30) * (2 / 40);  % V_OUT = 0V at -30dBm, 2V at
+10dBm

% Digital Output (D_OUT) Model: HIGH (1) if rf_dBm > -5 dBm

D_OUT = double(rf_dBm > -5);  % 1 = High, 0 = Low

% Plot the outputs

figure;

subplot(2,1,1);

plot(rf_dBm, V_OUT, 'b-', 'LineWidth', 2);

grid on;

title('Analog Output V_{OUT} vs RF Input Power');

xlabel('RF Input Power (dBm)');

ylabel('V_{OUT} (V)');

ylim([0 2.5]);

subplot(2,1,2);

stem(rf_dBm, D_OUT, 'r', 'LineWidth', 2);

grid on;

title('Digital Output D_{OUT} vs RF Input Power');

xlabel('RF Input Power (dBm)');

ylabel('D_{OUT} (Logic Level)');

ylim([-0.1 1.1]);
```